Analysis of earthquake-induced groundwater level change using self-organizing maps

Kei Nakagawa* · Zhi-Qiang Yu · Ronny Berndtsson · Makoto Kagabu

Kei Nakagawa (✉), Makoto Kagabu

Institute of Integrated Science and Technology, Nagasaki University,

1-14 Bunkyo-machi, Nagasaki 852-8521, Japan

e-mail: kei-naka@nagasaki-u.ac.jp

Tel.: +81 95 819 2763; fax: +81 95 819 2763

* corresponding author

Zhi-Qiang Yu

Graduate School of Fisheries and Environmental Sciences, Nagasaki University,

1-14 Bunkyo-machi, Nagasaki 852-8521, Japan

Ronny Berndtsson

Division of Water Resources Engineering & Center for Middle Eastern Studies, Lund University,

Box 118, SE-221 00 Lund, Sweden

Abstract

For a better understanding of possible physical links between geophysical observables and earthquake characteristics, it is important to analyze statistical spatiotemporal patterns in nature related to such events. For this purpose, characteristic changes in groundwater level (GWL) were observed before and after the 2016 Kumamoto earthquake in Japan. Previous research has shown that self-organizing maps (SOM) can be used to classify complex patterns of GWL-change during different parts of the earthquake sequence. In this study, we used before and after earthquake GWL data as input vectors to SOM. In total, 64 observed groundwater levels were classified into 12 different clusters. Most shallow wells displayed GWL difference that was small during the foreshock (first earthquake) and large during the main-shock (second earthquake). Upstream deep wells showed relatively large difference in water level from 1 to 2 days after the earthquakes. The GWL rapidly increased just after the earthquake, then tended to gradually decrease from September. Most of the shallow wells in the unconfined aquifer rapidly recovered to initial GWLs within several hours to several days, because of hydrostatic pressure. However, most of the deep wells in the confined aquifer needed longer time to recover, in some cases several weeks to several months. These findings are important for the physical understanding of earthquake effects on the groundwater environment, disaster prevention, and possibility for development of earthquake precursors.

Keywords

Kumamoto earthquake, Groundwater level (GWL) change, Self-organizing map (SOM), Cluster analysis

Introduction

The 2016 Kumamoto earthquake sequence started with a 6.2 M_W foreshock at 21:26 (JST) on April 14. About 28 hours later, it culminated in a 7.0 M_W main-shock tremor at 1:25 (JST) on April 16. The strike-slip movement of the seismogenic Hinagu-Futagawa fault is the main cause of this type of crustal earthquakes in the area. The earthquake triggered a series of natural disasters such as surface ruptures, landslides, land subsidence, liquefaction, which resulted in severe damage to infrastructure and buildings in the epicenter region, especially in Mashiki town and Minami-Aso village (Shirahama et al. 2016; Yamazaki and Liu 2016).

Hydrological effects occur simultaneously with seismic processes in earthquake-affected areas. Such effects may be liquefaction, groundwater level (GWL) anomalies, changes in water chemistry, formation or depletion of springs, streamflow variation, and eruption of mud volcanoes (Wang and Manga 2010; Manga and Wang 2015; Shi et al. 2015). During the last decades, with the development of efficient observation techniques, such phenomena are quantitatively recorded and analyzed for a better physical understanding, disaster prevention, and possible development of earthquake precursors (Roeloffs 1988; Tsunogai and Wakita 1995; Barberio et al. 2017). Especially, with respect to GWL effects, there have been many correlational studies. For example, (1) detailed observations of GWL-change types induced by one or multiple earthquakes (Chia et al. 2001, 2008; Cox et al. 2012; Shi et al. 2015), (2) mechanism assessment of GWL-change characteristics through interdisciplinary methods such as poroelastic theory, permeability enhancement, and undrained consolidated sediments (Wang and Chia 2008; Wang and Manga 2010; Manga and Wang 2015), and (3) numerical modeling using correlation between earthquake-triggered GWL-variation recovery and hydrogeological characteristics in different aquifers (Lin et al. 2018).

For an improved understanding of links between earthquakes and sub-surface hydrological processes, research has focused on the 2016 Kumamoto earthquake by applying various methods. Hosono et al. (2018) interpreted earthquake-induced structural deformation causing hydrologic response in the active volcanic system of the Mount Aso caldera. It clarified the source mechanism for new spring formation and assessment of hydrothermal solute fluxes by use of hydrogeochemistry, isotopes, and binary mixing calculations, respectively. Drinking water for habitants in the Kumamoto area is almost 100% from groundwater. Thus, this area has been equipped by a high-resolution and extensive monitoring system in groundwater wells for water quality, withdrawal, and hydrologic response to earthquakes. These data provide a unique opportunity to study how crustal earthquakes influence hydrological processes in the near-zone of earthquakes (within one rupture distance).

Recently, multivariate analysis using self-organizing maps (SOM) has been applied in various research fields, such as ecology, geomorphology, hydrology, meteorology, and wastewater treatment. SOM is an effective tool for studying and interpreting of spatiotemporally varying phenomena (Kalteh and Berndtsson 2007; Bedoya et al. 2009; Yu et al. 2014; Nguyen et al. 2014, 2015; Nakagawa et al. 2017; Yu et al. 2018). Using SOM, visual representation of complex but linked groundwater characteristics is possible. Ishihara et al. (2013) used SOM to evaluate GWL characteristics in Tokyo induced by the 2011 off the Pacific coast of Tohoku earthquake. Eight patterns were identified for the characteristics of unconfined and confined aquifer GWL-change. They concluded that SOM successfully characterized GWL fluctuation patterns affected by the earthquake.

In view of the above, this study deals with characteristic changes in GWL that were observed after the 2016 Kumamoto earthquake. The objectives are to improve the understanding regarding GWL effects due to seismic activities and give practical recommendations to groundwater supply managers regarding expected time scale of GWL changes in connection to earthquakes. For this purpose, SOM combined with hierarchical cluster analysis using before and after earthquake GWL data as input vectors are applied. The classification results obtained by the SOM analyses, the spatiotemporal properties of GWL-change, and seismic relationships are discussed in detail. The paper is closed by a discussion on practical advice to groundwater supply managers.

Materials and methods

Study area

Kumamoto area is located in the center of Kyushu Island, southern Japan. It occupies an area of 945 km^2. The main geology is constituted by Paleozoic bedrock of metamorphic and sedimentary rock, pre-Aso volcanic rock of Tertiary-Quaternary period, Quaternary Aso volcanic rock, and lacustrine alluvium. Pre-Aso volcanic rock has evolved as lava and tuff breccia. However, Quaternary Aso volcanic rocks are mainly pyroclastic deposits from four eruptions of the Aso volcano, named Aso-1 (270 ka), Aso-2 (140 ka), Aso-3 (120 ka), and Aso-4 (89 ka), respectively (Miyoshi et al. 2009; Hosono et al. 2013). These pyroclastic deposits as well as part of the alluvial deposits contain important aquifers. The uppermost Aso-4 and alluvial sediments include a near-surface unconfined aquifer with uneven thickness ranging from a few meters to 50 m. Aso-1, Aso-2, and Aso-3 contain confined aquifers with a varying thickness of 60-200 m. The discontinuous lacustrine deposits and marine sediments act as an aquiclude between the aquifers (Kagabu et al. 2017).

Locations of the 19 shallow and 45 deep wells acting as the monitoring system in this study is shown in **Fig. 1**. These monitoring wells are distributed over the Kumamoto groundwater area consisting of the Shirakawa and Midorikawa River watersheds. The regional climate is warm and humid. Mean annual temperature and precipitation are about 16.9℃ and 1986 mm, respectively. About 40% of the rainfall occur from June to July (Japan Meteorological Agency 2018).

Since groundwater is an important resource of the area, several correlational studies have been conducted such as combined use of isotopes for confirming nitrate origin (from chemical fertilizer, wastewater, and manure), attenuation mechanisms and identifying nitrate biogeochemical processes with regional groundwater flow (Hosono et al. 2013, 2014), evaluation of groundwater age by using multiple environmental tracers (Kagabu et al. 2017), and understanding the origin of fluoride, arsenic pollution, and cumulative environmental factors for groundwater quality (Hossain et al. 2016a, b). These studies have significantly contributed to groundwater quality protection and basis for policy decisions in the study area. At the same time, these studies provide an important background knowledge for a detailed understanding of groundwater processes in the area.

Self-organizing maps

Self-organizing maps (SOM) are powerful tools for spatiotemporal data analyses (Nguyen et al. 2015; Nakagawa et al. 2017). During recent decades SOM have been used in a multitude of research fields (e.g., Kalteh and Berndtsson 2007; Bedoya et al. 2009; Yu et al. 2014; Nguyen et al. 2014, 2015; Nakagawa et al. 2017; Yu et al. 2018). The advantage of SOM is that high-dimensional and complex data can be projected onto a more easily interpreted two-dimensional hexagonal array. Similarity of extracted SOM patterns is then compared visually using color gradients. The objective of SOM applications is to obtain useful and physically explainable reference vectors. The SOM properties also mean that a larger map size will give a higher resolution for pattern recognition. Optimal number of nodes and map configuration are determined by $m=5\sqrt{n}$, where m represents the number of map nodes and n the number of input data (Hentati et al. 2010). The number of rows and columns is dependent on the square root of the ratio between the two largest eigenvalues of transformed data (García and González 2004). These eigenvalues are calculated by principal component analysis (PCA). The reference vectors are obtained after iterative updates through a training phase that is composed by three main procedures: competition between nodes, selection of a winner node, and updating of the vectors. Results of the analysis are achieved after the training phase, which is fine-tuned using cluster analysis such as k-means algorithms (Jin et al. 2011). Davies-Bouldin Index (DBI), applying k-means algorithms, determines the optimal number of clusters (García and González 2004). In the present study, these calculations were made using a modified version of SOM Toolbox 2.0 (Vesanto et al. 2000).

Data

Six kinds of GWL data were used as input vectors to the SOM analyses. As mentioned above, the earthquake was composed of two shocks; foreshock (first earthquake) on April 14 and main-shock (second earthquake) on April 16. The GWL data were taken from the groundwater monitoring network at hourly auto-recorded time intervals and transferred to an administrative center. Before applying the SOM analysis, data were organized according to the sequence of foreshock and main-shock. The earthquake-affected GWL time sequences used in the analyses are shown in **Fig. 2.** According to Fig. 2, (1) GWL difference between before and after foreshock (April 14, 22:00 (B) - 21:00 (A)) denoted F(a): (B-A), (2) GWL difference between 22 hours and right after foreshock (April 15, 20:00 (C) - April 14, 22:00 (B)) denoted F(b): (C-B), (3) GWL difference between 2 days and 1 day after foreshock (average for April 16 (E) - April 15, 21:00 (D)) denoted F(c): (E-D), and (4) M(a) to M(c) are analogously defined as F(a) to F(c) as M(a): (G-F) GWL difference between before and after main-shock on April 16, 2:00 (G) - 1:00 (F). M(b): (H-G) is the GWL difference after 22 hours and right after main-shock on April 16, 23:00 (H) - 2:00 (G). M(c): (J-I) is the GWL difference between 2 days and 1 day after main-shock. The averaged GWL on April 18 (average) (J) - April 17, 1:00 (I). Using these defined six time series variables (F(a), F(b), F(c), M(a), M(b), and M(c)) served as input vectors to explore the spatiotemporal GWL-change characteristics for each observation location.

Results and discussion

Time series variation of reference vectors

The time series variation of reference vectors is shown in **Fig. 3**. The upper row represents the GWL change features during the foreshock, and the lower row shows the GWL change characteristics during the main-shock. A comparison between F(a) and F(b), M(a) and M(b), lower located neurons (reference vectors) displayed large GWL difference with a time lag of 22 hours. As well, F(b) and M(b) displayed a similar time variation. The behavior right after and 22 hours after the earthquakes was similar for both foreshock and main-shock. This means that both earthquakes had generally similar change characteristics for groundwater levels during this period (within 22 hours) for most of the monitoring wells. In addition, F(c) showed larger neuron changes than M(c). The reason for this is the superimposed effect of foreshock and main-shock for F(c). Besides using the defined six variables (F(a), F(b), F(c), M(a), M(b), and M(c)), the spatial variation characteristics of GWL difference are further explored in **Fig. 4**. The GWL change of M(a) is larger than F(a), because the main-shock formed a series of new faults and the increasing of seismic energy density. In addition, the GWL change of F(c) is also greater than M(c), as to the above discussion of superimposed effect. The general change characteristics of GWL difference is basically consistent with the SOM change features.

Cluster analysis

The cluster analysis using the SOM reference vectors resulted in 12 clusters as shown in **Fig. 5**. The number of clusters was determined through the DBI index as explained above. Accordingly, the minimum DBI corresponds to the optimal number of clusters, which was equal to 12 in this case. The number labeled for each reference vector corresponds to the number of observation wells classified into the vector. According to the dendrogram (**Fig. 6**), the number of parent clusters are 5 (distance of about 3.5). In this case, clusters 2 and 7, clusters 3, 4, 5, and 10, clusters 6, 9, and 12, clusters 8 and 11 are classified into the same parent groups. No well locations were classified into cluster 10. Thus, this cluster was excluded from further analysis. The unconfined aquifer wells were classified into clusters 1, 5, 9 and 11 that include 3, 7, 8, and 1 well, respectively. The main reason why we are not able to separate confined and unconfined wells before using SOM classification, is that unconfined well data are limited to only 19 wells.

Radar-charts of clusters

Radar-charts for each cluster display the main characteristics of the input data as displayed in **Fig. 7**. Cluster 1 is related to the downstream of Shirakawa and Midorikawa River watersheds 6 locations, F(b) and M(b) are quite small but on the other hand F(a) and M(a) are large. The GWL difference was small right after and 22 hours after the earthquake. The GWL difference was large before and after the earthquake.

Clusters 2 and 7 are related to the midstream basin well groups 1 and 3, respectively, which are represented by deep wells (F(b), M(b), and M(c) are large). This means that the GWL difference was large just after and 22 hours after both foreshock and main-shock. The GWL difference was as well large between 2 days and 1 day after the main-shock.

Clusters 3, 4, and 5 represent the mid- to downstream area with well groups 1, 2, and 14, respectively. F(c) and M(a) are quite large. The GWL difference between the 2nd and 1st day after foreshock was large (superimposed effect) and the GWL difference between before and after main-shock was large as well.

Clusters 6, 9, and 12 are related to the up- to midstream areas with well groups 3, 7, and 17, respectively. F(c) and M(c) were relatively large. The GWL difference between the 2nd and 1st day after the earthquakes was large.

Clusters 8 and 11 are related to both sides of the downstream to midstream area with 6 and 4 wells, respectively. F(a) and M(a) are small and F(b) and M(b) relatively large. The GWL difference before and after earthquakes was small, and relatively large just after and 22 hours after earthquakes.

According to the above, clusters 2 and 7, and clusters 6, 9, and 12 are areas that tend to sustain GWL change (M(c) is relatively large). These areas represent deep wells in the confined aquifer except for cluster 9. The mechanism for sustained GWL change is mainly from earthquake-enhanced permeability, because the transmission of pore pressure from the source to certain wells occurs with different distance and thus, needs different time. This is probably the reason why GWL response time is different from right after earthquake and 22 hours after as well as after 1 day and 2 days. The degree of GWL change is probably influenced by well depth, hydrogeological characteristics, and seismic frequency. This indicates very complex geophysical relationships. Generally, different clusters represent different GWL response in terms of time difference from seismic waves and degree of change. Looking at the case when M(a) is larger than F(a) (clusters 5, 6, 8, 9, and 11), the degree of GWL change may be affected by earthquake magnitude under similar hypocentral distance (fault location of inducing foreshock and main-shock is closer) (Wang and Chia 2008). This is due to the fact that seismic energy density increases with larger earthquake magnitude.

GWL-change related to clusters

In order to analyze GWL-change characteristics for each cluster, the data were standardized using maximum and minimum of the change according to:

$$\bar{h} = \frac{h - h_{min}}{h_{max} - h_{min}}$$

where h is GWL, h_{max} and h_{min} are maximum and minimum GWL, respectively, and $\bar{h}$ is standardized GWL. To explore annual variation patterns of GWL change for each cluster, the time scale of data was set to one year. Unfortunately, 8 out the 64 wells did not have a full year record as the earthquake caused a power failure and disruption of data recording for these wells. Thus, we used the remaining 56 wells for the following analyses. The obtained similar well clusters and mean GWL are shown in **Fig. 8**. In order to discriminate between earthquakes GWL-change from other GWL-change factors (such as precipitation evaporation, air temperature, and transpiration effects, recharge and withdrawal, etc.), ten year averages of GWL are used as background value in each cluster in Fig. 8.

For cluster 1 (5 wells), a general GWL decline occurred in April and August, the GWL tends to return to its initial state. Compared to the ten-year average, the drop of GWL in April is clearly explained by the earthquakes (foreshock and main-shock). The drop of GWL in August was due to the unusually small precipitation during this month. The GWL declined 0.17 m in April as compared to the ten-year average.

For cluster 2 (1 well) and 7 (3 wells), the earthquake delayed the general GWL recovery due to increasing rainfall. The maximum GWL drop occurred in May and continued until June. After this, GWL recovered due to rainfall. However, the earthquake effects continued to sustain a low GWL and it did not recover to average levels as seen in cluster 2. This is consistent with the assessment from the radar-charts. For clusters 2 and 7, the GWL decreased 0.69 m and 0.13 m in May compared to the ten-year average, respectively.

In the case of cluster 3 (1 well), 4 (2 wells), and 5 (13 wells), the general GWL decline occurred in April and August similar to cluster 1. For cluster 3, the GWL decline continued until December and did not recover to the initial level. The GWL reduced by 0.55 m in December compared to the ten-year average. However, for clusters 4 and 5, the GWL gently increased after the earthquakes, then gradually tended to return to initial level. The tendency of GWL recovery from summer to winter is similar to the 10-year average GWL variation. In the same manner, cluster 4 and 5, display April GWLs in the same range as the ten-year average (0.03 m and 0.01 m, respectively).

For cluster 6 (3 wells), 9 (14 wells), and 12 (5 wells), the GWL variation is similar to the general pattern of the 10-year average. However, the effect of the earthquakes is still noticeable. After the initial drop due to the earthquake, the GWL rapidly increased just after the earthquake and then tended to gradually decrease from September. Obviously, these clusters had higher GWL after the earthquake than before. All wells in cluster 6 and 12 are deep and located along the upstream-mountain sides. The rapidly increasing GWLs may be the results of the contribution of mountain-hold groundwater. For cluster 6 and 12, the GWL change exceeded 0.54 m to 2.94 m and 0.1 m to 2.19 m as compared to the ten-year average during April to September, respectively. As well, cluster 9 also increased 0.1 m to 0.48 m from April to September.

In the case of cluster 8 (6 wells), GWL decline occurred in April, then slowly increased after the earthquake. The GWL tended to return back to initial levels in August, as well as continuously increase up to October. For cluster 8, the GWL varied from -0.11 m to 0.47 m during April to August as compared to the ten-year average.

For cluster 11 (3 wells), the GWL decline occurred from April to June, then gradually increased from July to October. The GWL did not recover to initial levels. This is clear, when comparing to the 10-year average GWL change. For cluster 11, the GWL declined 0.16 m to 0.17 m from April to June compared to the ten-year average. In these clusters (8 and 11), the GWL peak occurred in October. This peak is also shown in the GWL change for the past ten-year average.

Most of the shallow wells in the unconfined aquifer rapidly recovered to initial GWLs within several hours to several days. This was due to hydrostatic pressure. However, most of the deep wells in the confined aquifer needed longer time to recover, in some cases several weeks to several months. According to Shi et al. (2015), co-seismic GWL-change usually prevails more than one week after the earthquake. On the contrary, co-seismic GWL-change shorter than one week is a transient change. From the annual variation characteristics such as for clusters 2, 7, and 11 (deep wells except for only one well), the GWL-decline seems to be sustained over 1-3 months. Shallow wells such as cluster 1, 5, and 9 were also affected by extremely low rainfall in August. Even if two wells in cluster 4 are deep wells, GWL dropped in August. They were probably affected by adjacent shallow wells.

Spatial distribution of clusters

The spatial distribution of clusters is shown in **Fig. 9**. Spatial distribution of clusters is reasonably logically arranged, meaning that wells belonging to the same clusters are located at similar locations. A vast majority of the shallow wells are classified into cluster 5 (downstream) and 9 (midstream). These general cluster characteristics pertain a before and after GWL difference that was large for the main-shock, but small for the foreshock. After the earthquake, the GWL-change was comparatively small and finally returned back to initial levels. Some of the deep wells are classified into cluster 6 and 12 (upstream-mountainside). These general cluster characteristics involve relatively large GWL difference 2 days and 1day after both foreshock and main-shock. As these wells are located on the mountainside, the rapid rise in GWL was probably fed by mountain-originating groundwater affected by tremor. Due to this, the GWL change was sustained several weeks to several months.

Conclusions

To explore transient spatiotemporal variation characteristics in GWL-change induced by earthquakes, SOM was used. As a conclusion, 64 observation wells were classified into 12 different clusters. Most shallow wells were classified into cluster 5 and 9. These groups were represented by a GWL difference that was small during the foreshock (first earthquake) and large during the main-shock (second earthquake). The GWL gently increased after the earthquake, then tended to stabilize around the initial level. Upstream deep wells were classified into cluster 6 and 12. This group showed relatively large difference in water level from 1 to 2 days after the earthquakes. The GWL rapidly increased just after the earthquake, then tended to gradually decrease from September. Cluster 1 displayed small difference in water level just after and 22 hours after the earthquake.

The observed wells could be clearly classified into 12 clusters. This information can be used by local governments and water supply managers to better plan appropriate groundwater management in case of a coming earthquake. For example, cluster 1 shows earthquake effects in April but the GWL recovered by December. Consequently, it may be expected that groundwater levels will return to normal within a year.

In the case of cluster 2 and 7, the GWL did not recover to initial levels and the earthquake effects continued for a long period. Thus, large groundwater withdrawal from these wells may need to halt for several years to protect water resources. In the case of cluster 3, 4, and 5, we need to continue GWL monitoring until recovery can be seen, because GWL did not recover to initial levels. However, in the case of cluster 6, 9, and 12, GWL increased compared to the 10-year average due to the contribution of mountain-hold water. Consequently, these wells can be used for emergency demand.

The findings in this paper have improved the physical understanding on how earthquakes affect the groundwater environment. It is as well important to understand how earthquakes may affect the chemical quality of the drinking water supply. Thus, in future research, we will extend the analyses to longer timescales for GWL change as affected by earthquakes and in addition include groundwater chemistry in the analyses (Cox et al. 2012; Shi et al. 2015).

Acknowledgements This work was financially supported by JSPS KAKENHI under Grant No. JP17H01861 and SUNTORY Kumamoto groundwater research project.

References

Bedoya D, Novotny V, Manolakos ES (2009) Instream and offstream environmental conditions and stream biotic integrity. Importance of scale and site similarities for learning and prediction. Ecol Modell 220:2393-2406. doi: 10.1016/j.ecolmodel.2009.06.017

Barberio MD, Barbieri M, Billi A, Doglioni C, Petitta M (2017) Hydrogeochemical changes before and during the 2016 Amatrice-Norcia seismic sequence (central Italy). Sci Rep7:1-12. doi: 10.1038/s41598-017-11990-8

Cox SC, Rutter HK, Sims A, Manga M, Weir JJ, Ezzy T, White PA, Horton TW, Scott D (2012) Hydrological effects of the M_W 7.1 Darfield (Canterbury) earthquake, 4 September 2010, New Zealand. New Zeal J Geol Geophys 55:231-247. doi: 10.1080/00288306.2012.680474

Chia Y, Chiu JJ, Chiang YH, Lee TP, Liu CW (2008) Spatial and temporal changes of groundwater level induced by thrust faulting. Pure Appl Geophys 165:5-16. doi: 10.1007/s00024-007-0293-5

Chia Y, Wang YS, Chiu JJ, Liu CW (2001) Changes of groundwater level due to the 1999 Chi-Chi earthquake in the Choshui River alluvial fan in Taiwan. Bull Seismol Soc Am 91:1062-1068. doi: 10.1785/0120000726

García HL, González IM (2004) Self-organizing map and clustering for wastewater treatment monitoring. Eng Appl Artif Intell 17:215-225. doi: 10.1016/j.engappai.2004.03.004

Hentati A, Kawamura A, Amaguchi H, Iseri Y (2010) Evaluation of sedimentation vulnerability at small hillside reservoirs in the semi-arid region of Tunisia using the Self-Organizing Map.

Geomorphology 122:56-64. doi: 10.1016/j.geomorph.2010.05.013

Hosono T, Hartmann J, Louvat P, Amann T, Washington KE, West AJ, Okumura K, BÖttcher ME, Gaillardet J (2018) Earthquake-induced structural deformations enhance long-term solute fluxes from active volcanic systems. Sci Rep 8:14809. doi: 10.1038/s41598-018-32735-1

Hosono T, Tokunaga T, Kagabu M, Nakata H, Orishikida T, Lin IT, Shimada J (2013) The use of $\delta^{15}N$ and $\delta^{18}O$ tracers with an understanding of groundwater flow dynamics for evaluating the origins and attenuation mechanisms of nitrate pollution. Water Res 47:2661-2675. doi: 10.1016/j.watres.2013.02.020

Hosono T, Tokunaga T, Tsushima A, Shimada J (2014) Combined use of $\delta^{13}C$, $\delta^{15}N$, and $\delta^{34}S$ tracers to study anaerobic bacterial processes in groundwater flow systems. Water Res 54:284-296. doi: 10.1016/j.watres.2014.02.005

Hossain S, Hosono T, Ide K, Matsunaga M, Shimada J (2016a) Redox processes and occurrence of arsenic in a volcanic aquifer system of Kumamoto Area, Japan. Environ Earth Sci 75:1-19. doi: 10.1007/s12665-016-5557-x

Hossain S, Hosono T, Yang H, Shimada J (2016b) Geochemical processes controlling fluoride enrichment in groundwater at the western part of Kumamoto Area, Japan. Water Air Soil Pollut 227:385.

doi: 10.1007/s11270-016-3089-3

Ishihara S, Kawamura A, Amaguchi H, Takasaki T, Kawai M (2013) Evaluation of characteristics of groundwater level fluctuation in Tokyo by the 2011 off the Pacific coast of Tohoku Earthquake using self-organizing maps. Journal of Japan Society of Civil Engineers, Ser. BI (Hydraulic Engineering) 69(4): I_541-I_546.

Japan Meteorological Agency (2018) Weather observation data. Japan Meteorological Agency Web. http://www.jma.go.jp/jma/index.html. Accessed 16 November 2018

Jin YH, Kawamura A, Park SC, Nakagawa N, Amaguchi H, Olsson J (2011) Spatiotemporal classification of environmental monitoring data in the Yeongsan River basin, Korea, using self-organizing maps. J Environ Monit 13: 2886-2894.

doi: 10.1039/c1em10132c

Kagabu M, Matsunaga M, Ide K, Momoshima N, Shimada J (2017) Groundwater age determination using ^{85}Kr and multiple age tracers (SF_6, CFCs, and ^{3}H) to elucidate regional groundwater flow systems. J Hydrol Reg Stud 12:165-180.

doi: 10.1016/j.ejrh.2017.05.003

Kalteh AM, Berndtsson R (2007) Interpolating monthly precipitation by self-organizing map (SOM) and multilayer perceptron (MLP). Hydrol Sci J 52:305-317.

doi: 10.1623/hysj.52.2.305

Kohonen T (2001) Self-organizing maps, 3rd edn. Springer, Berlin

Liu C-Y, Chia Y, Chuang P-Y, Chiu Y-C, Tseng T-L (2018) Impacts of hydrogeological characteristics on groundwater-level changes induced by earthquakes. Hydrogeol J 26:451-465. doi: 10.1007/s10040-017-1684-z

Miyoshi M, Furukawa K, Shinmura T, Shimono M, Hasenaka T, (2009) Petrography and whole-rock geochemistry of pre-Aso lavas from the caldera wall of Aso volcano, central Kyushu. Journal of the Geological Society of Japan 115:672-687 (in Japanese with English abstract). https://doi.org/10.5575/geosoc.115.672

Nakagawa K, Amano H, Kawamura A, Berndtsson R (2017) Classification of groundwater chemistry in Shimabara, using self-organizing maps. Hydrol Res 48:840-850. https://doi.org/10.2166/nh.2016.072

Nguyen TT, Kawamura A, Tong TN, Nakagawa N, Amaguchi H, Gilbuena R (2014) Spatial classification of grovundwater monitoring data in the Red River Delta, Vietnam using self-organizing maps. Annual Journal of Hydraulic Engineering, JSCE 70(4): I_241-I_246. https://doi.org/10.2208/jscejhe.70.I_241

Nguyen TT, Kawamura A, Tong TN, Nakagawa N, Amaguchi H, Gilbuena R (2015) Clustering spatio-seasonal hydrogeochemical data using self-organizing maps for groundwater quality assessment in the Red River Delta, Vietnam. J Hydrol 522: 661-673. doi: 10.1016/j.jhydrol.2015.01.023

Roeloffs EA (1988) Hydrologic precursors to earthquakes: A review. Pure Appl Geophys PAGEOPH 126:177-209.
doi: 10.1007/BF00878996

Shirahama Y, Yoshimi M, Awata Y, Maruyama T, Azuma T, Miyashita Y, Mori H, Imanishi K, Takeda N, Ochi T, Otsubo M, Asahina D, Miyakawa A (2016) Characteristics of the surface ruptures associated with the 2016 Kumamoto earthquake sequence, central Kyushu, Japan. Earth, Planets Sp 68:1-12.
doi: 10.1186/s40623-016-0559-1

Shi Z, Wang G, Manga M, Wang CY (2015) Mechanism of co-seismic water level change following four great earthquakes-insights from co-seismic responses throughout the Chinese mainland. Earth and Planet Sci Lett 430:66-74.
doi: 10.1016/j.epsl.2015.08.012

Tsunogai U, Wakita H (1995) Precursory chemical changes in ground water: Kobe earthquake, Japan. Science 269:61-63.
doi: 10.1126/science.269.5220.61

Vesanto J, Himberg J, Alhoniemi E, Parahankangas J (2000) SOM Toolbox for Matlab 5, Helsinki University of Technology Report A57

Wang CY, Chia Y (2008) Mechanism of water level changes during earthquakes: Near field versus intermediate field. Geophys Res Lett 35:1-5. doi: 10.1029/2008GL034227

Wang CY, Manga M (2010) Hydrologic responses to earthquakes and a general metric. Front Geofluids 206-216. doi: 10.1002/9781444394900.ch14

Manga M, Wang C-Y (2015) Earthquake Hydrology. In: Gerald Schubert (ed), Treatise on Geophysics, 2nd edn. Vol 4. Elsevier, Oxford, pp 305-328

Yamazaki F, Liu W (2016) Remote sensing technologies for post-earthquake damage assessment: a case study on the 2016 Kumamoto earthquake. 6th ASIA Conference on Earthquake Engineering, At Cebu City, Philippines.

Yu H, Song Y, Liu R, Pan H, Xiang L, Qian F (2014) Identifying changes in dissolved organic matter content and characteristics by fluorescence spectroscopy coupled with self-organizing map and classification and regression tree analysis during wastewater treatment. Chemosphere 113: 79-86. doi: 10.1016/j.chemosphere.2014.04.020

Yu ZQ, Amano H, Nakagawa K, Berndtsson R (2018) Hydrogeochemical evolution of groundwater in a Quaternary sediment and Cretaceous sandstone unconfined aquifer in Northwestern China. Environ Earth Sci 77: 629. doi: 10.1007/s12665-018-7816-5

Figure Captions

Figure 1 Monitoring wells in the Kumamoto area

Figure 2 GWL-change in representative wells in connection to the Kumamoto earthquake sequence. (A-J indicate point-in-time to calculate water level variation before and after foreshock and main-shock. By using point-in-time (A-J), six variables were defined as F(a):(B-A), F(b):(C-B), F(c):(E-D), M(a):(G-F), M(b):(H-G), and M(c):(J-I), respectively)

Figure 3 Component planes for (F(a), F(b), F(c), M(a), M(b), and M(c))

Figure 4 Spatial distribution characteristics of GWL difference by use of the six variables (F(a), F(b), F(c), M(a), M(b), and M(c))

Figure 5 Visualized map of the twelve clusters by the SOM

Figure 6 Dendrogram for respective group using node numbers of SOM

Figure 7 Radar-chart for each cluster

Figure 8 Annual variation pattern for mean GWL of each cluster

Figure 9 Cluster classification for Kumamoto monitoring wells

Figure 1

Click here to access/download;Figure;Fig1.tiff

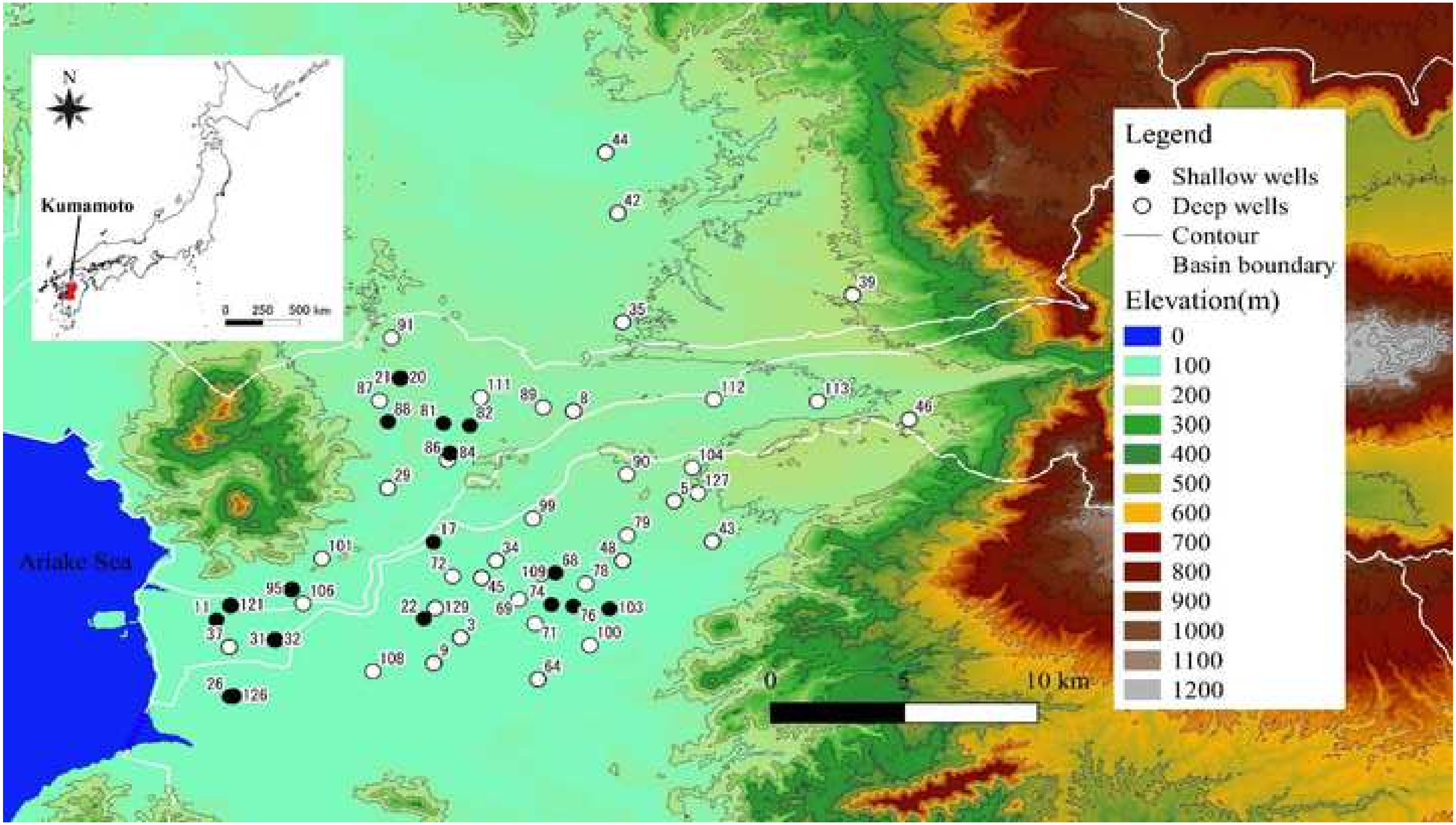

Figure 2

Click here to access/download;Figure;Fig2.tiff

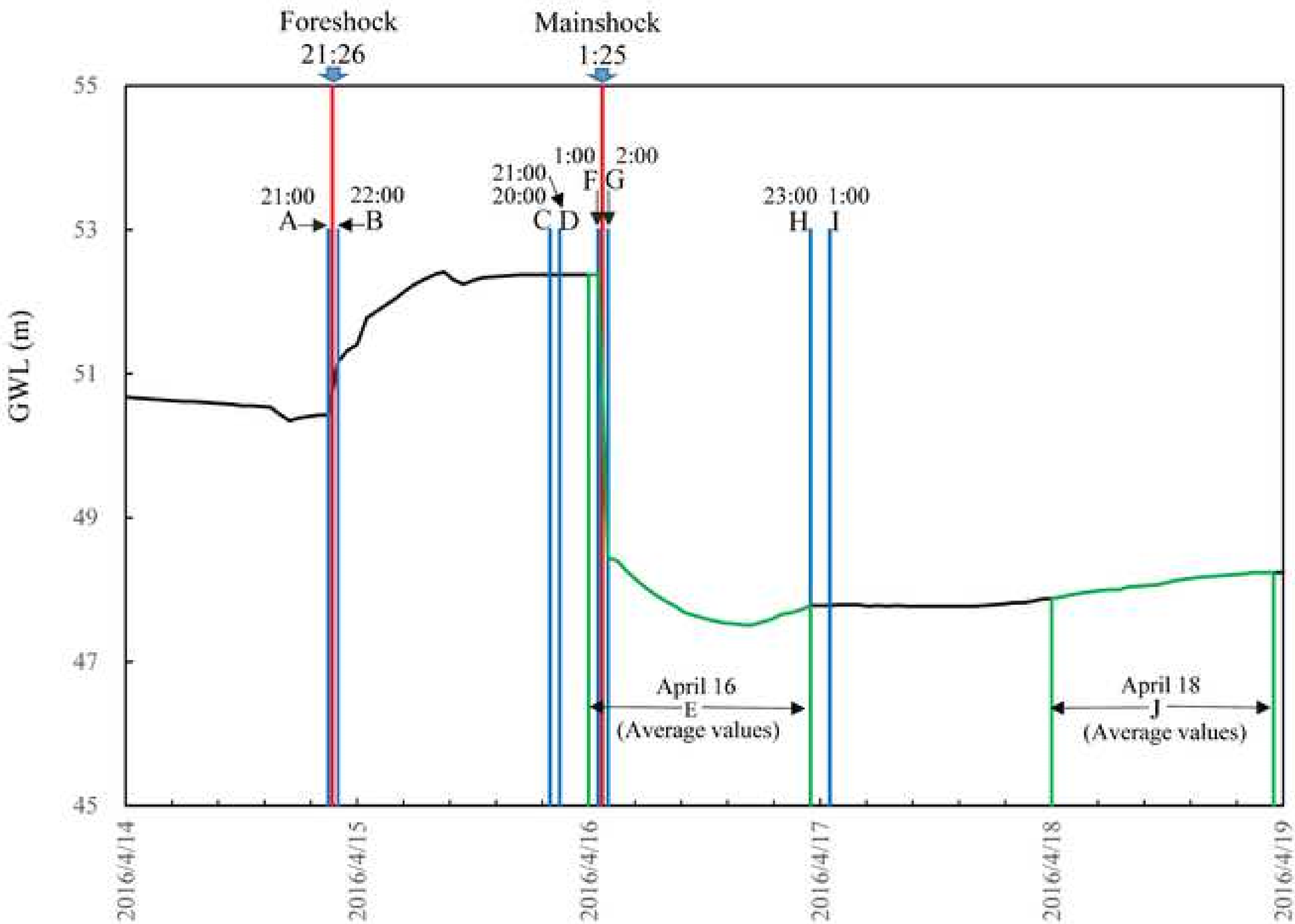

Figure 3

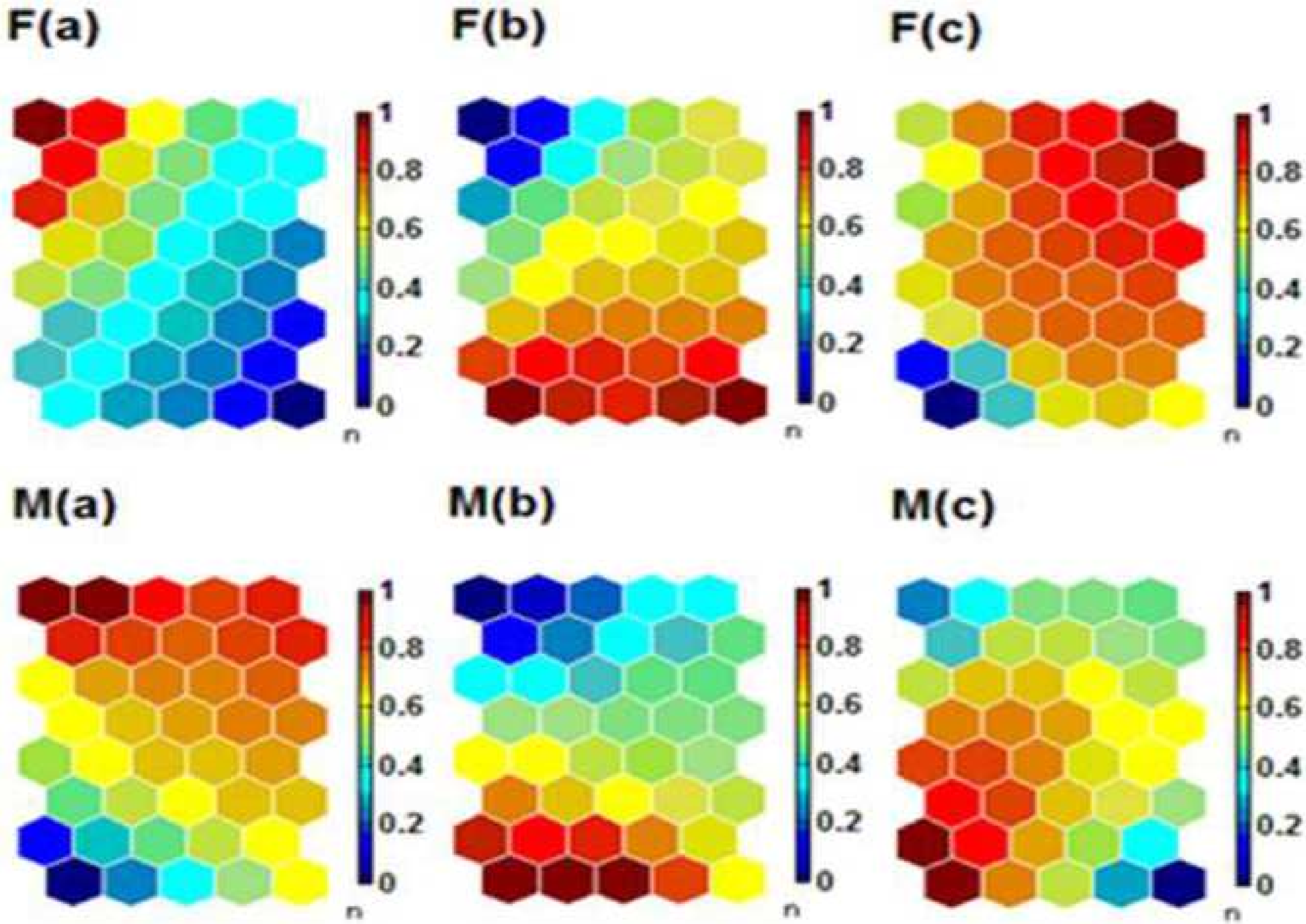

Figure 4 Click here to access/download;Figure;Fig4.tiff

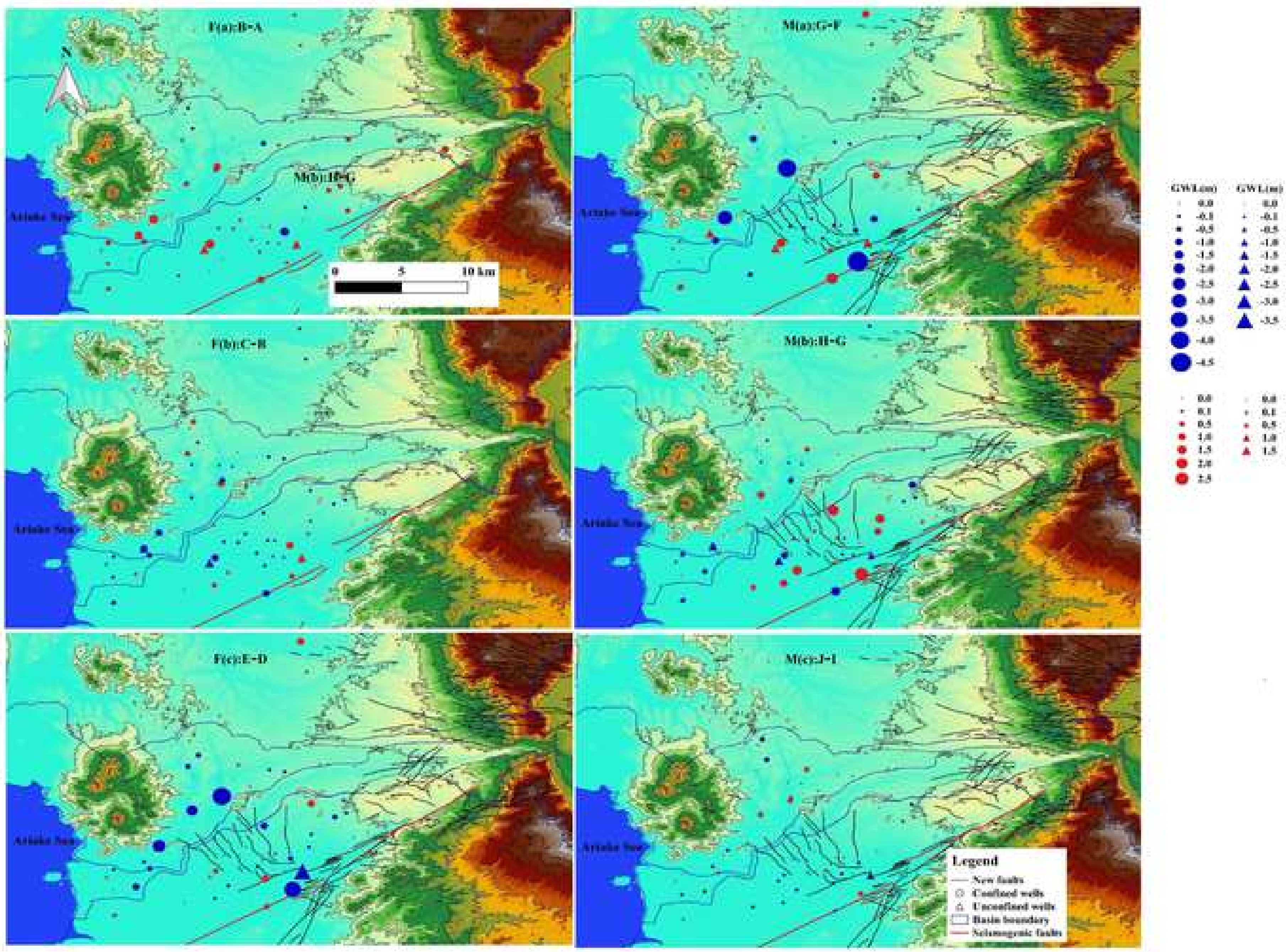

Figure 5 Click here to access/download;Figure;Fig5.tiff

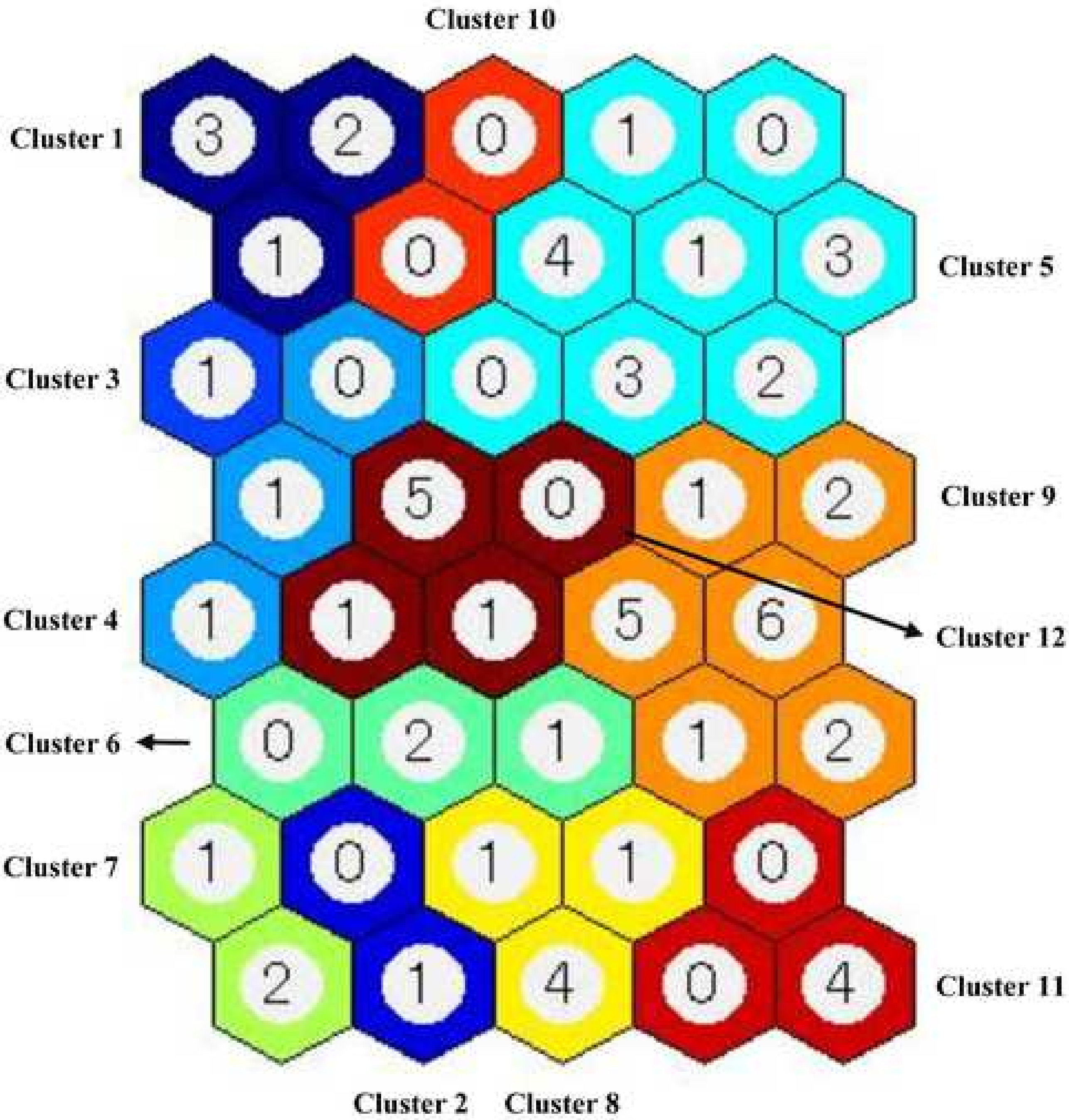

Figure 6

Click here to access/download;Figure;Fig6(1).tiff

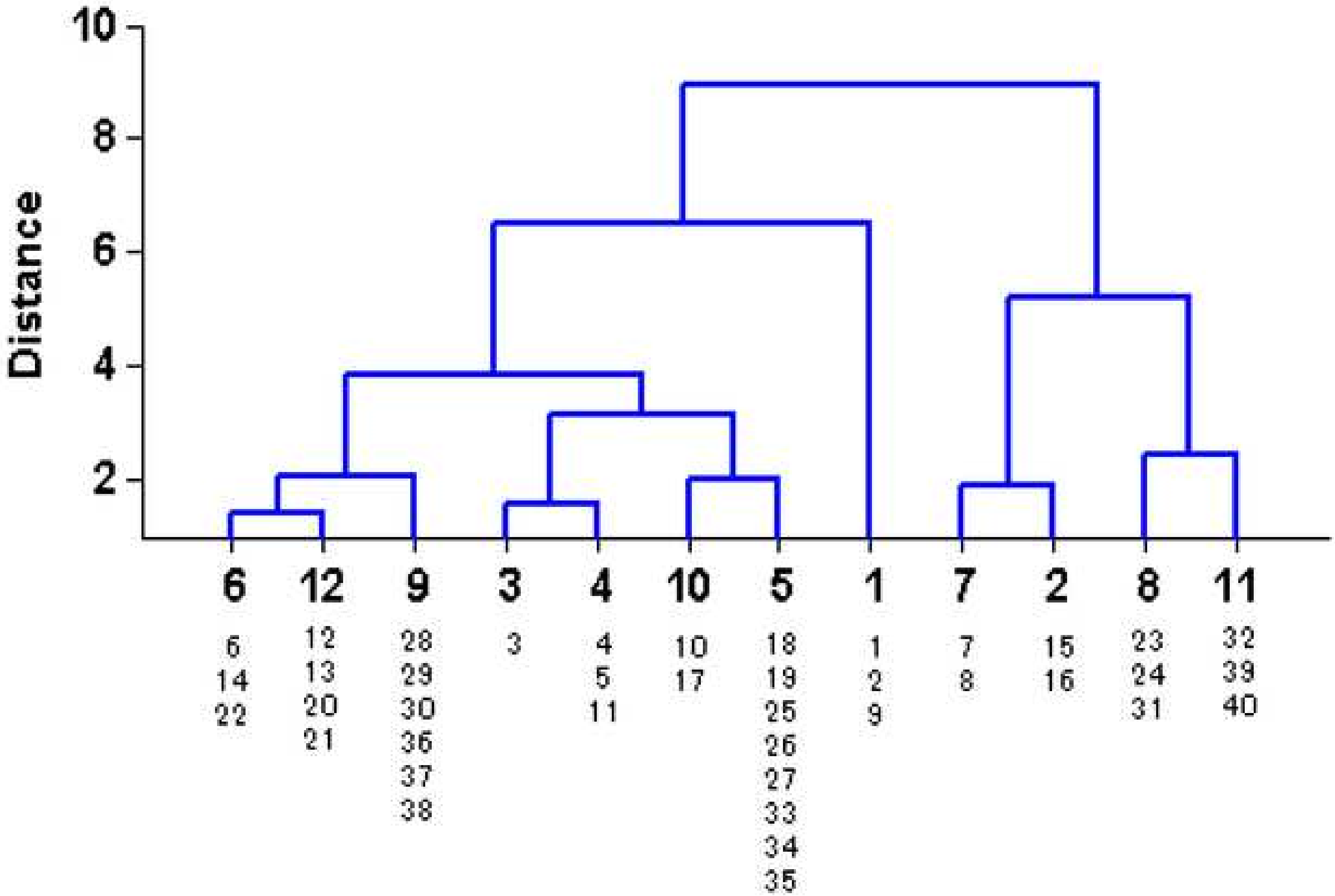

Figure 7

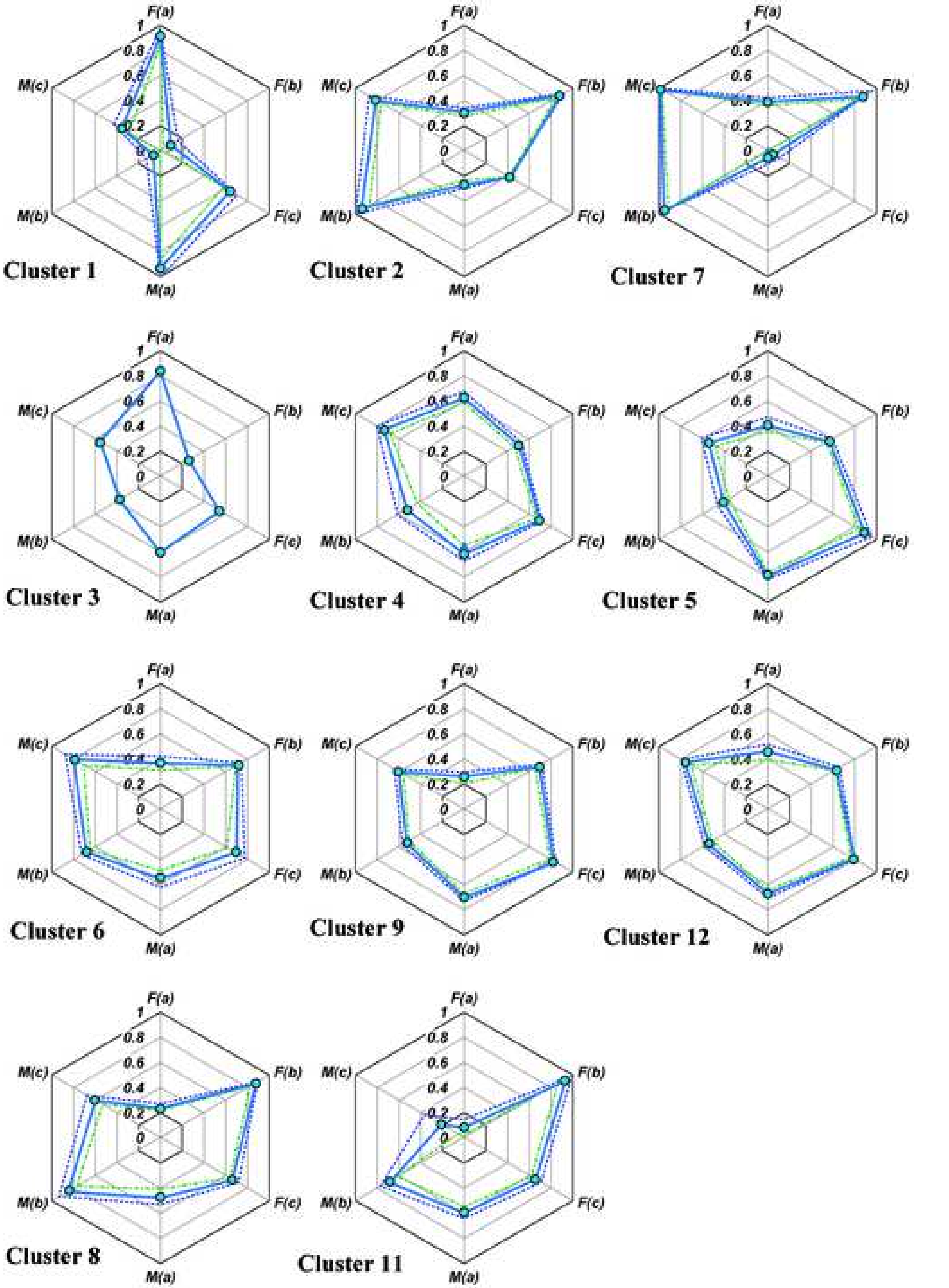
F(a)
F(b)
F(c)
M(a)
M(b)
M(c)
1
0.8
0.6
0.4
0.2
0
Cluster 1
Cluster 2
Cluster 7
Cluster 3
Cluster 4
Cluster 5
Cluster 6
Cluster 9
Cluster 12
Cluster 8
Cluster 11

Figure 8

Click here to access/download;Figure;Fig8.tiff

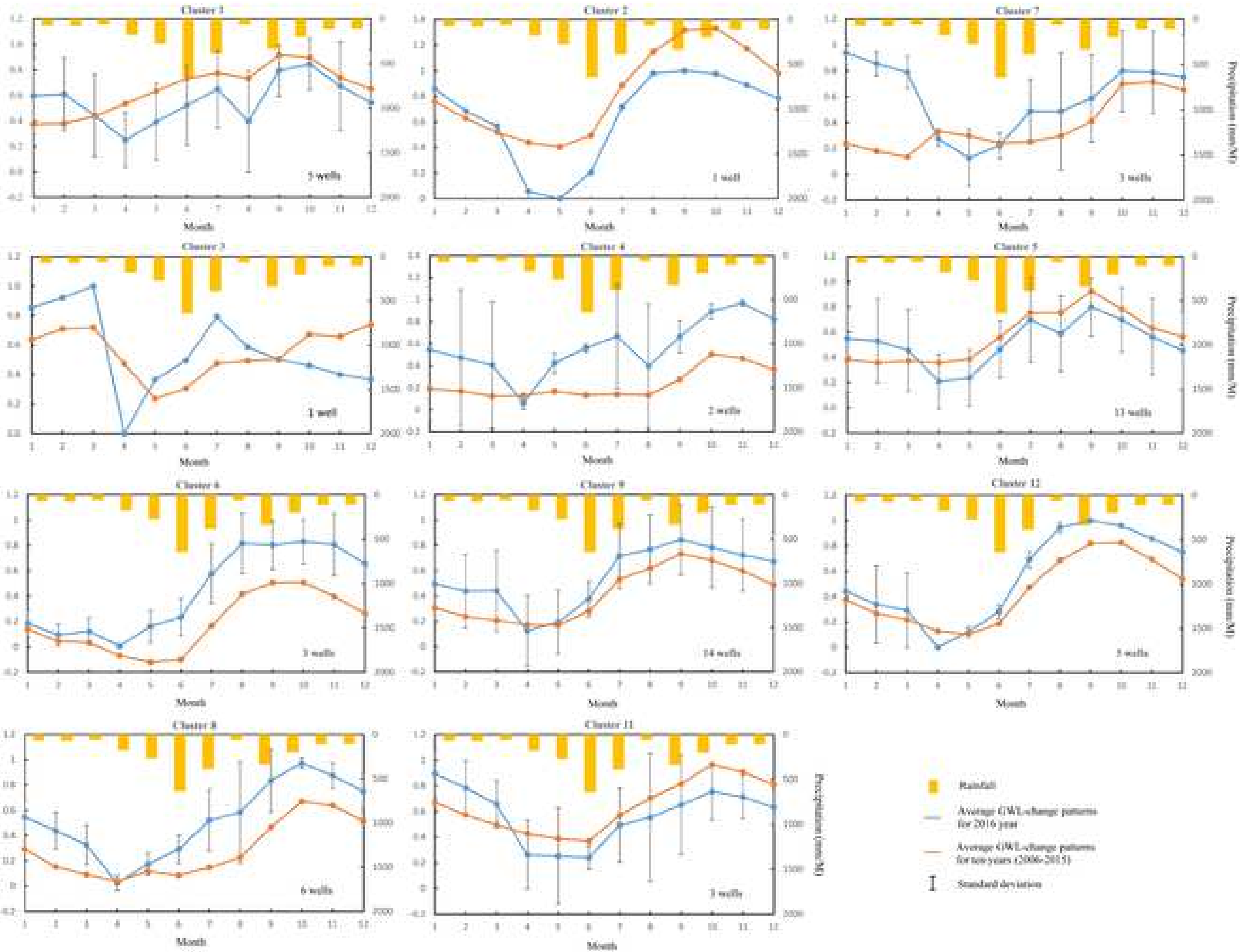

Figure 9

Click here to access/download;Figure;Fig9.tiff